Available online at www.sciencedirect.com
ScienceDirect
Journal of Magnetic Resonance 185 (2007) 28–37
JMR Journal of Magnetic Resonance
www.elsevier.com/locate/jmr

On the application of magic echo cycles for quadrupolar echo spectroscopy of spin-1 nuclei

E.S. Mananga [a,b], R. Roopchand [a], Y.S. Rumala [a], G.S. Boutis [a,*]

[a] York College, The City University of New York, Department of Natural Sciences, Physics, 94-20 Guy R. Brewer Boulevard, Jamaica, NY 11451, USA
[b] The Graduate Center of The City University of New York, OEODP, 365 Fifth Avenue, New York, NY 10016-4309, USA

Received 24 July 2006; revised 19 September 2006
Available online 30 November 2006

Abstract

Magic echo cycles are introduced for performing quadrupolar echo spectroscopy of spin-1 nuclei. An analysis is performed via average Hamiltonian theory showing that the evolution under chemical shift or static field inhomogeneity can be refocused simultaneously with the quadrupolar interaction using these cycles. Due to the higher convergence in the Magnus expansion, with sufficient RF power, magic echo based quadrupolar echo spectroscopy outperforms the conventional two pulse quadrupolar echo in signal to noise. Experiments highlighting a signal to noise enhancement over the entire bandwidth of the quadrupolar pattern of a powdered sample of deuterated polyethelene are shown.

Keywords: Quadrupolar echo; Finite pulse widths; Deuterium NMR; Magic echo; Average Hamiltonian theory

1. Introduction

One of the most intriguing effects in nuclear magnetic resonance is the refocusing of the time evolution of a nuclear spin system with a suitable RF pulse cycle—the creation of a spin echo. In the language of average Hamiltonian theory, developed by Waugh and coworkers, the refocusing of a spin system occurs when the effective Hamiltonian of a given pulse train is zero [1]. This can be illustrated by considering the evolution of the initial state of a spin, $|\psi(t=0)\rangle$, to the final state $|\psi(t=T)\rangle$ under the effective Hamiltonian, H_{eff}. When H_{eff} is made zero by clever design of the RF pulse train, the state at $t=T$ is made equal to that at $t=0$, and the dynamics have been refocused. For quadrupolar spins of a solid, a spin echo allows for spectroscopy of a broad spectral pattern that would otherwise be distorted due to the ring-down of the RF coil. The experimental method involves acquiring the peak of an echo, which in the absence of relaxation and experimental artifacts, would yield the same signal as a free induction decay.

Arguably the most challenging experimental requirement to overcome in quadrupolar echo spectroscopy of a solid is the uniform excitation of the entire bandwidth of the spin system, which can often cover 200 kHz. Composite pulses developed for this purpose were shown to produce more uniformly excited spectra than spectra acquired with a conventional hard pulse (a single pulse with a single phase and amplitude) [2]. Under certain experimental conditions, however, the spectrum acquired with a composite pulse was shown by Siminovich et al. to produce a distortions due to finite pulse width artifacts [3]. This was due to the fact that the spin system evolves under the quadrupolar interaction during the RF pulses. In the situation of hard pulses, a similar distortion is also encountered even when one uses high power and short pulses on the order of 2 μs. Recently, we reported on a phase cycling scheme that suppresses spectral artifacts associated with finite pulse width effects in a conventional quadrupolar echo cycle [4]. By proper cycling of the transmitter and receiver phases, distortions introduced by finite pulse widths were

* Corresponding author. Fax: +1 718 262 2652.
E-mail address: gboutis@york.cuny.edu (G.S. Boutis).

1090-7807/$ - see front matter © 2006 Elsevier Inc. All rights reserved.
doi:10.1016/j.jmr.2006.10.016

shown to be significantly suppressed to first order of the Magnus expansion.

In this work, we report on the application of magic echoes for improved quadrupolar echo spectroscopy of spin $I=1$ nuclei. The magic echo cycle, developed by Rhim et al. [5] nearly 36 years ago, has been applied with great success in solid state NMR imaging [6–8], scattering studies [9,10] and in multiple pulse line-narrowing schemes [11]. A particularly useful aspect of the cycles presented is their ability to refocus both chemical shift and static field inhomogeneity simultaneous with the quadrupolar interaction. In addition, with sufficient RF power, the signal to noise over the entire bandwidth is enhanced in a magic echo cycle compared to the familiar two pulse quadrupolar echo cycle due to more efficient convergence of the Magnus expansion. Lastly, the magic echo based cycles are shown to be robust against finite pulse width artifacts that plague other cycles used in quadrupolar echo spectroscopy. In the experimental section of this work, we demonstrate these findings on a sample of powdered deuterated polyethelene.

2. Theory

Consider a solid system of spin $I=1$ nuclei subject to a large, static and homogeneous field. Ignoring any dipolar coupling and chemical shift, the nuclear spin Hamiltonian is given by the familiar quadrupolar interaction, which is written to first order as

$$H_{\omega_Q} = \omega_Q[12I_{z,1}I_{z,1} - II] \tag{1}$$

where the spin-1 operator formalism developed by Vega and Pines has been used [12]. In the above expression

$$\begin{aligned}\omega_Q &= \omega'_Q R_{2,0}\frac{1}{\sqrt{6}}\\ R_{2,0} &= \sqrt{\frac{3}{2}}\left[P_2(\cos\theta) + \left(\frac{\eta}{2}\right)\cos(2\theta)\sin^2(\varphi)\right]\\ \omega'_Q &= \frac{e^2qQ}{2I(2I-1)\hbar}\end{aligned} \tag{2}$$

where ω_Q is the quadrupolar coupling constant, $P_2(\cos\theta)$ is the second order Legendre polynomial of $\cos\theta$, θ and φ are two of the three Euler angles.

We consider the evolution of the spin system under the magic echo pulse sequence shown in Fig. 1, developed by Rhim et al. [5]. The cycle is already well known in the NMR community to refocus the dynamics of spin $I=1/2$ nuclei coupled by a dipolar interaction as well as chemical shift or offset Hamiltonians [11]. The sequence consists of a $\frac{\pi}{2}$ pulse about x axis, a period of free evolution of time $\tau-\alpha$, a $\frac{\pi}{2}$ pulse about y axis, followed by two spin locking fields of duration $2\tau-\alpha$, ending with the application of a second $\frac{\pi}{2}$ pulse about y axis. The echo occurs at a time $\tau-\alpha$ after the last pulse [5]. Table 1 lists all 16 possible cycles of a magic echo sequence that create an echo. In Table 1, the numbers 0, 1, 2 and 3 correspond to the transmitter or receiver phases X, Y, $-X$ and $-Y$, respectively. The phase of the receiver in each cycle is set so that the echo is always detected on either the positive x or y axis.

In the formalism of average Hamiltonian theory, the time evolution of the system from time $t=0$, $\rho(0)$ to the state at time $t=t_c$, $\rho(t_c)$ is given by

$$\rho(t_c) = U_{RF}U_{int}\rho(0)U_{int}^{-1}U_{RF}^{-1} \tag{3}$$

where the propagator U_{RF} is given by the Dyson series and U_{int} is given by the Magnus expansion [1]. This formalism will be used to show that the magic echo cycle is more robust in refocusing the dynamics of spin-1 nuclei coupled by a quadrupolar interaction compared to the conventional two pulse echo cycle shown in Fig. 2 with sufficient RF power. In addition, the magic echo cycle refocuses static field inhomogeneity and chemical shift simultaneous with the quadrupolar interaction.

Taking the initial state of the system to be given by $\rho(0)=I_{z,1}$, we constructed Table 2 and computed the toggling frame quadrupolar Hamiltonian $\widetilde{H}_{\omega_Q}$ during each stage of the pulse cycle. Referring to Fig. 1, for the first time interval $0\leqslant t\leqslant\tau-2\alpha$, $U_{RF}=1$. For the second interval, $\tau-2\alpha\leqslant t\leqslant\tau$, the rotation is given by the linear parametrization:

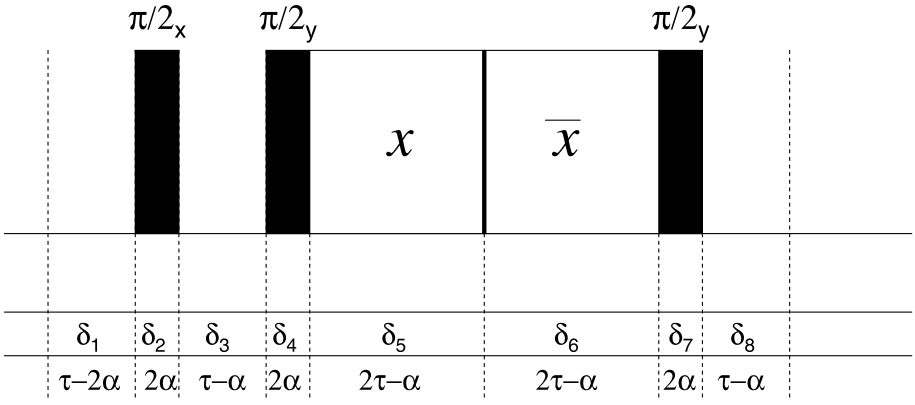

Fig. 1. Magic echo sequence for refocusing the quadrupolar, chemical shift Hamiltonian as well as static field inhomogeneity. In this figure, the two $\pi/2$ pulses have a width of 2α and the phases of all the pulses should be cycled as given in Table 1 to suppress deleterious spectral artifacts. The cycle shown is cycle A from Table 1.

Table 1
Phase cycling table for the magic echo cycle for use in the spin-1 quadrupolar echo experiment

Cycle	A	B	C	D	E	F	G	H	I	J	K	L	M	N	O	P
Pulse 1	0	0	0	0	1	1	1	1	2	2	3	3	2	2	3	3
Pulse 2	1	3	0	2	0	2	1	3	1	3	1	3	0	2	0	2
Pulse 3	0	0	1	1	1	1	0	0	0	0	0	0	1	1	1	1
Pulse 4	2	2	3	3	3	3	2	2	2	2	2	2	3	3	3	3
Pulse 5	1	3	0	2	0	2	1	3	1	3	1	3	0	2	0	2
Receiver phase	3	3	1	1	0	0	2	2	1	1	0	0	3	3	2	2

Fig. 1 shows cycle A from the table above.

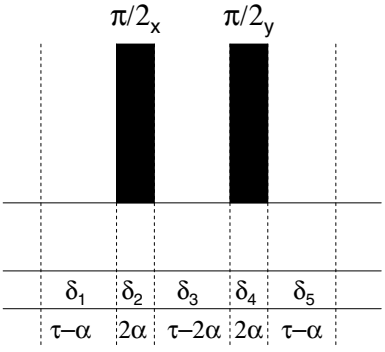

Fig. 2. Two pulse echo sequence for refocusing the quadrupolar Hamiltonian. In the figure the two π/2 pulses have a width of 2α and the phases of the two pulses shown can be any combination of 90 deg phase shifted pulses. The cycle does not refocus chemical shift or static field in homogeneity.

$$\theta = \omega_{\mathrm{RF}} t \tag{4}$$

with the constraint

$$\omega_{\mathrm{RF}} 2\alpha = \frac{\pi}{2} \tag{5}$$

where $\theta = 0$ at $t = 0$, and $\theta = \frac{\pi}{2}$ at $t = 2\alpha$. The same condition occurs for the fourth and seventh interval respectively, $2\tau - \alpha \leqslant t \leqslant 2\tau + \alpha$ and $6\tau - \alpha \leqslant t \leqslant 6\tau + \alpha$. For the fifth and sixth intervals, $2\tau + \alpha \leqslant t \leqslant 4\tau$ and $4\tau \leqslant t \leqslant 6\tau - \alpha$, the parametrization is given by the constraint

$$(2\tau - \alpha)\omega_{\mathrm{RF}} = n\pi \tag{6}$$

with $n = 1, 2, 3\ldots$. In the experimental section, we will comment on how precise this condition is required to be set by the experimenter in order for the cycles to function properly.

Table 2 gives the toggling frame Hamiltonians during each stage of the system evolution that were developed knowing the transformations of $I_{x,1}$, $I_{y,1}$ and $I_{z,1}$. The resulting toggling frame Hamiltonians were integrated over their respective time intervals and are also provided in Table 2. The zeroth order terms of the Magnus expansion were calculated for all 16 cycles that can refocus the system dynamics evolving under Eq. (1), and produce an echo and are provided in Table 3.

Consider the case of magic echo cycle denoted by A in Table 1 and shown in Fig. 1. From Table 3 the zeroth order term of the Magnus expansion is given by

Table 2
Transformations of the operator U_{RF} and the toggling frame quadrupolar Hamiltonian during each stage of the magic echo sequence shown in Fig. 1

Interval	Time	U_{RF}	$\tilde{H}_{\omega_{\mathrm{Q}}}$
δ_1	$0 < t \leqslant \tau - 2\alpha$	1	$\omega_{\mathrm{Q}}[12I_{z,1}I_{z,1} - \Pi]$
δ_2	$\tau - 2\alpha < t \leqslant \tau$	$\exp[2i\theta(t)I_{x,1}]$	$\omega_{\mathrm{Q}}[12I_{z,1}I_{z,1}\cos^2(\theta) + 12I_{y,1}I_{y,1}\sin^2(\theta) + 12I_{z,2}\cos(\theta)\sin(\theta) - \Pi]$
δ_3	$\tau < t \leqslant 2\tau - \alpha$	$\exp[i\pi I_{x,1}]$	$\omega_{\mathrm{Q}}[12I_{y,1}I_{y,1} - \Pi]$
δ_4	$2\tau - \alpha < t \leqslant 2\tau + \alpha$	$\exp[2i\theta(t)I_{y,1}]\times\exp[i\pi I_{x,1}]$	$\omega_{\mathrm{Q}}[12I_{y,1}I_{y,1}\cos^2(\theta) + 12I_{x,1}I_{x,1}\sin^2(\theta) - 12I_{z,2}\cos(\theta)\sin(\theta) - \Pi]$
δ_5	$2\tau + \alpha < t \leqslant 4\tau$	$\exp[2i\theta(t)I_{x,1}]\times\exp[i\pi I_{y,1}]\times\exp[i\pi I_{x,1}]$	$\omega_{\mathrm{Q}}[12I_{x,1}I_{x,1}\cos^2(\theta) + 12I_{z,1}I_{z,1}\sin^2(\theta) + 12I_{y,2}\cos(\theta)\sin(\theta) - \Pi]$
δ_6	$4\tau < t \leqslant 6\tau - \alpha$	$\exp[-2i\theta(\xi)I_{x,1}]\times\exp[2i\theta(\xi)I_{x,1}]\times\exp[i\pi I_{y,1}]\times\exp[i\pi I_{x,1}]$	$\omega_{\mathrm{Q}}[12I_{x,1}I_{x,1}\cos^2(\omega_{\mathrm{RF}}(t-\xi)) + 12I_{z,1}I_{z,1}\sin^2(\omega_{\mathrm{RF}}(t-\xi)) - 12I_{y,2}\cos(\omega_{RF}(t-\xi))\sin(\omega_{\mathrm{RF}}(t-\xi)) - \Pi]$
δ_7	$6\tau - \alpha < t \leqslant 6\tau + \alpha$	$\exp[2i\theta(t)I_{y,1}]\times\exp[i\pi I_{y,1}]\times\exp[i\pi I_{x,1}]$	$\omega_{\mathrm{Q}}[12I_{x,1}I_{x,1}\cos^2(\theta) + 12I_{y,1}I_{y,1}\sin^2(\theta) + 12I_{z,2}\cos(\theta)\sin(\theta) - \Pi]$
δ_8	$6\tau + \alpha < t \leqslant 7\tau$	$\exp[2i\pi I_{y,1}]\times\exp[i\pi I_{x,1}]$	$\omega_{\mathrm{Q}}[12I_{y,1}I_{y,1} - \Pi]$

In this table $\xi = 2\tau - \alpha$, $\omega_{\mathrm{Q}} = \omega'_{\mathrm{Q}} R_{2,0}\frac{1}{\sqrt{6}}$ and $\omega'_{\mathrm{Q}} = \frac{e^2qQ}{2\hbar(2I-1)\hbar}$.

Table 3
Integrated first order terms of the Magnus expansion for the quadrupolar Hamiltonian for 16 cycles of the magic sandwich based quadrupolar echo sequence in Fig. 1

Cycle	$\overline{H}^0_{\omega_Q}$
A	$\frac{3}{7\tau}\frac{\omega_Q}{\omega_{RF}}I_{x,2}+\frac{4\tau\omega_Q}{7\tau}I_{x,1}I_{x,1}+\frac{4(3\alpha-\tau)\omega_Q}{7\tau}I_{x,1}+\frac{4(3\alpha-\tau)\omega_Q}{7\tau}I_{y,1}I_{y,1}+\frac{4(3\alpha+\tau)\omega_Q}{7\tau}I_{z,1}I_{z,1}$
B	$\frac{3}{7\tau}\frac{\omega_Q}{\omega_{RF}}I_{x,2}+\frac{4(3\alpha-\tau)\omega_Q}{7\tau}[I_{x,1}I_{x,1}+I_{y,1}I_{y,1}-2I_{z,1}I_{z,1}]$
C	$\frac{3}{7\tau}\frac{\omega_Q}{\omega_{rf}}I_{x,2}+\frac{8\tau\omega_Q}{7\tau}I_{z,1}I_{z,1}+\frac{4(3\alpha-\tau)\omega_Q}{7\tau}I_{y,1}I_{y,1}+\frac{4(3\alpha+\tau)\omega_Q}{7\tau}I_{x,1}I_{x,1}$
D	$\frac{3}{7\tau}\frac{\omega_Q}{\omega_{rf}}I_{x,2}+\frac{8\tau\omega_Q}{7\tau}I_{z,1}I_{z,1}+\frac{4(3\alpha-\tau)\omega_Q}{7\tau}I_{y,1}I_{y,1}+\frac{4(3\alpha+\tau)\omega_Q}{7\tau}I_{x,1}I_{x,1}$
E	$\frac{-3}{7\tau}\frac{\omega_Q}{\omega_{rf}}I_{y,2}+\frac{4(3\alpha-\tau)\omega_Q}{7\tau}[I_{x,1}I_{x,1}+I_{y,1}I_{y,1}-2I_{z,1}I_{z,1}]$
F	$\frac{-3}{7\tau}\frac{\omega_Q}{\omega_{rf}}I_{y,2}+\frac{4(3\alpha-\tau)\omega_Q}{7\tau}[I_{x,1}I_{x,1}+I_{y,1}I_{y,1}-2I_{z,1}I_{z,1}]$
G	$\frac{-3}{7\tau}\frac{\omega_Q}{\omega_{RF}}I_{y,2}+\frac{8\tau\omega_Q}{7\tau}I_{z,1}I_{z,1}+\frac{4(3\alpha-\tau)\omega_Q}{7\tau}I_{x,1}I_{x,1}-\frac{4(3\alpha+\tau)\omega_Q}{7\tau}I_{y,1}I_{y,1}$
H	$\frac{-3}{7\tau}\frac{\omega_Q}{\omega_{rf}}I_{y,2}+\frac{4(3\alpha-\tau)\omega_Q}{7\tau}[I_{x,1}I_{x,1}+I_{y,1}I_{y,1}]+\frac{8\tau\omega_Q}{7\tau}I_{z,1}I_{z,1}$
I	$\frac{-3}{7\tau}\frac{\omega_Q}{\omega_{rf}}I_{y,2}+\frac{4(3\alpha-\tau)\omega_Q}{7\tau}[I_{x,1}I_{x,1}+I_{y,1}I_{y,1}]+\frac{8\tau\omega_Q}{7\tau}I_{z,1}I_{z,1}$
J	$\frac{-3}{7\tau}\frac{\omega_Q}{\omega_{rf}}I_{y,2}+\frac{4(3\alpha-\tau)\omega_Q}{7\tau}[I_{x,1}I_{x,1}+I_{y,1}I_{y,1}-2I_{z,1}I_{z,1}]$
K	$\frac{3}{7\tau}\frac{\omega_Q}{\omega_{rf}}I_{y,2}+\frac{8\tau\omega_Q}{7\tau}I_{z,1}I_{z,1}+\frac{4(3\alpha-\tau)\omega_Q}{7\tau}I_{x,1}I_{x,1}-\frac{4(3\alpha+\tau)\omega_Q}{7\tau}I_{y,1}I_{y,1}$
L	$\frac{3}{7\tau}\frac{\omega_Q}{\omega_{rf}}I_{y,2}+\frac{8\tau\omega_Q}{7\tau}I_{z,1}I_{z,1}+\frac{4(3\alpha-\tau)\omega_Q}{7\tau}I_{x,1}I_{x,1}-\frac{4(3\alpha+\tau)\omega_Q}{7\tau}I_{y,1}I_{y,1}$
M	$\frac{-3}{7\tau}\frac{\omega_Q}{\omega_{rf}}I_{x,2}-\frac{4(3\alpha+\tau)\omega_Q}{7\tau}I_{x,1}I_{x,1}+\frac{4(3\alpha-\tau)\omega_Q}{7\tau}I_{y,1}I_{y,1}+\frac{8\tau\omega_Q}{7\tau}I_{z,1}I_{z,1}$
N	$\frac{-3}{7\tau}\frac{\omega_Q}{\omega_{rf}}I_{x,2}-\frac{4(3\alpha+\tau)\omega_Q}{7\tau}I_{x,1}I_{x,1}+\frac{4(3\alpha-\tau)\omega_Q}{7\tau}I_{y,1}I_{y,1}+\frac{8\tau\omega_Q}{7\tau}I_{z,1}I_{z,1}$
O	$\frac{3}{7\tau}\frac{\omega_Q}{\omega_{rf}}I_{y,2}+\frac{4(3\alpha-\tau)\omega_Q}{7\tau}[I_{x,1}I_{x,1}+I_{y,1}I_{y,1}]+\frac{8\tau\omega_Q}{7\tau}I_{z,1}I_{z,1}$
P	$\frac{3}{7\tau}\frac{\omega_Q}{\omega_{rf}}I_{y,2}+\frac{4(3\alpha-\tau)\omega_Q}{7\tau}[I_{x,1}I_{x,1}+I_{y,1}I_{y,1}]+\frac{8\tau\omega_Q}{7\tau}I_{z,1}I_{z,1}$

In this table $2\omega_{RF}\alpha=\frac{\pi}{2}$, where 2α is the $\frac{\pi}{2}$ pulse width. ω_Q is the quadrupolar coupling constant.

$$\overline{H}^0_{\omega_Q}=\frac{1}{7\tau}\frac{12\alpha\omega_Q}{\pi}I_{x,2}+\frac{4(3\alpha-\tau)}{7\tau}\omega_Q[I_{x,1}I_{x,1}+I_{y,1}I_{y,1}-2I_{z,1}I_{z,1}] \tag{7}$$

Three important findings of this result should be recognized. First, the second term commutes with $I_{z,1}$, and as a consequence does not affect the system dynamics. Second, the first term is proportional to the finite pulse width and when $\alpha\to 0$ the first term vanishes. In this situation, the density matrix at $t=7\tau$, calculated using Eq. (3), is found to be $\rho_A(7\tau)=I_{y,1}$, which corresponds to the case of perfect refocusing of the spin system with no additional quantum coherences present to first order of the Magnus expansion. Third, the results indicate that the contribution of finite pulse widths to the system evolution becomes less important for large values τ.

To further illustrate the contribution of finite pulse widths in the system evolution, we consider Eq. (3) with Eq. (7) to determine the state of the spin system at 7τ and the detected signal. The density matrix at 7τ for the magic echo cycle A is found to be

$$\begin{aligned}\rho_A(7\tau)=&-2A_{11}\cos\left(\frac{3b}{8}\right)I_{z,2}-2A_{11}\sin\left(\frac{3b}{8}\right)I_{z,1}\\&+\left[A_{21}\cos\left(\frac{3b}{8}\right)+A_{31}\sin\left(\frac{3b}{8}\right)\right]I_{y,1}\\&+\left[-A_{31}\cos\left(\frac{3b}{8}\right)+A_{21}\sin\left(\frac{3b}{8}\right)\right]I_{y,2}\end{aligned} \tag{8}$$

where

$$\begin{aligned}A_{11}&=\frac{2a\sinh\left[\frac{1}{8}\sqrt{-16a^2-9b^2}\right]}{\sqrt{-16a^2-9b^2}}\\A_{21}&=\cosh\left[\frac{1}{8}\sqrt{-16a^2-9b^2}\right]\\A_{31}&=\frac{3b\sinh\left[\frac{1}{8}\sqrt{-16a^2-9b^2}\right]}{\sqrt{-16a^2-9b^2}}\end{aligned} \tag{9}$$

and $a=3\frac{\omega_Q}{\omega_{RF}}$ and $b=4(3\alpha-\tau)\omega_Q$.

In the limiting case when $\alpha=0$, the result above reduces to $\rho_A(7\tau)=I_{y,1}$. This is in agreement with our expectation in the situation of δ-function RF pulses. When $\alpha\neq 0$ the term $I_{y,2}$ does not commute with the quadrupolar Hamiltonian and as a consequence, it evolves to a detectable signal. In certain experimental conditions, it can produce a spectral distortion as we will now show. Using the Liouville–Von Neumann equation, the quadrupolar Hamiltonian in Eq. (1) and $\rho_A(7\tau)$, the density matrix at a time $t+7\tau$ is found to be

$$\begin{aligned}\rho_A(t+7\tau)=&-2A_{11}\cos\left(\frac{3b}{8}\right)I_{z,2}-2A_{11}\sin\left(\frac{3b}{8}\right)I_{z,1}\\&+\left[\left(A_{21}\cos\left(\frac{3b}{8}\right)+A_{31}\sin\left(\frac{3b}{8}\right)\right)\cos(3\omega_Q t)\right.\\&\left.+\left(A_{21}\sin\left(\frac{3b}{8}\right)-A_{31}\cos\left(\frac{3b}{8}\right)\right)\sin(3\omega_Q t)\right]I_{y,1}\\&+\left[\left(-A_{21}\cos\left(\frac{3b}{8}\right)-A_{31}\sin\left(\frac{3b}{8}\right)\right)\sin(3\omega_Q t)\right.\\&\left.+\left(A_{21}\sin\left(\frac{3b}{8}\right)-A_{31}\cos\left(\frac{3b}{8}\right)\right)\cos(3\omega_Q t)\right]I_{y,2}\end{aligned} \tag{10}$$

The signal detected for this cycle as a function of time is formally given by

$$\text{Signal}_A(7\tau+t)=\text{Trace}\{(I_{x,1}+iI_{y,1})\rho_A(7\tau+t)\} \tag{11}$$

which reduces to

$$\begin{aligned}&\text{Signal}_A(7\tau+t)\\&=i\left[\left(A_{21}\cos\left(\frac{3b}{8}\right)+A_{31}\sin\left(\frac{3b}{8}\right)\right)\right.\\&\quad\times\cos(3\omega_Q t)+\left(A_{21}\sin\left(\frac{3b}{8}\right)\right.\\&\quad\left.\left.-A_{31}\cos\left(\frac{3b}{8}\right)\right)\sin(3\omega_Q t)\right]\\&\quad\times Trace\{I_{y,1}(I_{x,1}+iI_{y,1})\}\end{aligned} \tag{12}$$

In the expression for $\rho_A(t+7\tau)$, the term $[(A_{21}\cos(\frac{3b}{8})+A_{31}\sin(\frac{3b}{8}))\cos(3\omega_Q t)+(A_{21}\sin(\frac{3b}{8})-A_{31}\cos(\frac{3b}{8}))\sin(3\omega_Q t)]$ multiplying $I_{y,1}$ arises from the time evolution of the terms $I_{y,1}$ and $I_{y,2}$ in $\rho_A(7\tau)$. The term $\cos(3\omega_Q t)$ arises from the time evolution of the term $I_{y,1}$ and is an even function.

The term $\sin(3\omega_Q t)$ arises from the time evolution of the term $I_{y,2}$ and is an odd function that vanishes in the case of delta function RF pulses ($\alpha = 0$). The detected signal, which is the term multiplying $I_{y,1}$, is a combination of odd and even functions. The sum of odd and even functions produces a slightly asymmetric spectrum, which causes one of the peaks of the quadrupolar powder pattern to be higher than the other. This finding was also reported recently for a conventional solid echo in spin-1 quadrupolar echo spectroscopy [4]. The asymmetry vanishes in the limit of $\alpha \to 0$.

If a strong RF field is applied to the spin system, the undesirable terms can be made negligible and Eq. (8) will be proportional to $I_{y,1}$. For example, a readily achievable pulse width of $2\alpha = 2\,\mu s$ with $\omega_Q = 125\,kHz$ and $\tau = 50\,\mu s$ under the magic echo cycle generates an $I_{y,1}$ term approximately 2 orders of magnitude larger than $I_{y,2}$. With higher RF power these deleterious terms can be made further negligible. A similar calculation can be performed for the other cycles given in Table 1.

The density matrices at 7τ for all 16 possible combinations of phase shifted RF pulses were calculated and are provided in Table 3, each highlighting the effect of ω_{RF} on the system evolution. We add or subtract the density matrices of all eight possible combinations of the ME cycles that produce an echo in the $+X$ direction in the following manner

$$\rho_{X\text{Total}} = \rho_E + \rho_F + \rho_K + \rho_L - \rho_M - \rho_G - \rho_O - \rho_P \tag{13}$$

where $\rho_{i=E,\ F,\ K,\ldots}$ is the density matrices for each cycle shown in Table 3. Using the results in Table 3, Eq. (13) reduces to

$$\begin{aligned}\rho_{X\text{Total}} = \Bigg[&-4A_{21}\cos\left(\frac{3b}{8}\right) - 4A_{33}\cos\left(\frac{b}{8}\right) - 4A_{33}\cos\left(\frac{2c}{8}\right)\\ &-4A_{33}\cos\left(\frac{d}{8}\right) - 4A_{31}\sin\left(\frac{3b}{8}\right) + 4A_{32}i\cos\left(\frac{b}{8}\right)\\ &+4A_{32}i\cos\left(\frac{c}{4}\right) + 4A_{32}i\cos\left(\frac{d}{8}\right)\Bigg]I_{x,1}\\ &+\Bigg[4A_{21}\sin\left(\frac{3b}{8}\right) - 4A_{33}\sin\left(\frac{b}{8}\right) + 4A_{33}\sin\left(\frac{2c}{8}\right)\\ &-4A_{33}\sin\left(\frac{d}{8}\right) - 4_{31}\cos\left(\frac{3b}{8}\right) + 4A_{32}i\sin\left(\frac{b}{8}\right)\\ &-4A_{32}i\sin\left(\frac{c}{4}\right) + 4A_{32}i\sin\left(\frac{d}{8}\right)\Bigg]I_{x,2}\end{aligned} \tag{14}$$

where a, b, c, d, A_{11}, A_{21}, A_{31} and A_{33} are given in Table 4.

Table 4
Density matrices at 7τ, $\rho(7\tau)$, for 16 cycles of the magic sandwich based quadrupolar echo pulse sequence for a system evolving under the first order secular quadrupolar Hamiltonian

Cycle	$\rho(7\tau)$
A	$-2A_{11}\cos(\frac{3b}{8})I_{z,2} - 2A_{11}\sin(\frac{3b}{8})I_{z,1} + [A_{21}\cos(\frac{3b}{8}) + A_{31}\sin(\frac{3b}{8})]I_{y,1} + [A_{21}\sin(\frac{3b}{8}) - A_{31}\cos(\frac{3b}{8})]I_{y,2}$
B	$-2A_{11}\cos(\frac{3b}{8})I_{z,2} - 2A_{11}\sin(\frac{3b}{8})I_{z,1} + [A_{21}\cos(\frac{3b}{8}) + A_{31}\sin(\frac{3b}{8})]I_{y,1} + [A_{21}\sin(\frac{3b}{8}) - A_{31}\cos(\frac{3b}{8})]I_{y,2}$
C	$-2A_{12}\cos(A_0)I_{z,2} + 2A_{12}\sin(A_0)I_{z,1} + [-A_{22}\cos(A_0) + A_{32}\sin(A_0)]I_{y,1} + [A_{32}\cos(A_0) + A_{22}\sin(A_0)]I_{y,2}$
D	$-2A_{12}\cos(A_0)I_{z,2} + 2A_{12}\sin(A_0)I_{z,1} + [-A_{22}\cos(A_0) + A_{32}\sin(A_0)]I_{y,1} + [A_{32}\cos(A_0) + A_{22}\sin(A_0)]I_{y,2}$
E	$2A_{11}\cos(\frac{3b}{8})I_{z,2} - 2A_{11}\sin(\frac{3b}{8})I_{z,1} - [A_{21}\cos(\frac{3b}{8}) + A_{31}\sin(\frac{3b}{8})]I_{x,1} - [-A_{21}\sin(\frac{3b}{8}) + A_{31}\cos(\frac{3b}{8})]I_{x,2}$
F	$2A_{11}\cos(\frac{3b}{8})I_{z,2} - 2A_{11}\sin(\frac{3b}{8})I_{z,1} - [A_{21}\cos(\frac{3b}{8}) + A_{31}\sin(\frac{3b}{8})]I_{x,1} + [A_{21}\sin(\frac{3b}{8}) - A_{31}\cos(\frac{3b}{8})]I_{x,2}$
G	$2A_{12}\cos(A_0)I_{z,2} + 2A_{12}\sin(A_0)I_{z,1} + [A_{22}\cos(A_0) - A_{32}\sin(A_0)]I_{x,1} + [A_{32}\cos(A_0) + A_{22}\sin(A_0)]I_{x,2}$
H	$2A_{12}\cos(A_0)I_{z,2} + 2A_{12}\sin(A_0)I_{z,1} + [A_{22}\cos(A_0) - A_{32}\sin(A_0)]I_{x,1} + [A_{32}\cos(A_0) + A_{22}\sin(A_0)]I_{x,2}$
I	$-2A_{11}\cos(\frac{3b}{8})I_{z,2} - 2A_{11}\sin(\frac{3b}{8})I_{z,1} - [A_{21}\cos(\frac{3b}{8}) + A_{31}\sin(\frac{3b}{8})]I_{y,1} + [-A_{21}\sin(\frac{3b}{8}) + A_{31}\cos(\frac{3b}{8})]I_{y,2}$
J	$-2A_{11}\cos(\frac{3b}{8})I_{z,2} - 2A_{11}\sin(\frac{3b}{8})I_{z,1} - [A_{21}\cos(\frac{3b}{8}) + A_{31}\sin(\frac{3b}{8})]I_{y,1} + [-A_{21}\sin(\frac{3b}{8}) + A_{31}\cos(\frac{3b}{8})]I_{y,2}$
K	$2A_{12}\cos(A_0)I_{z,2} + 2A_{12}\sin(A_0)I_{z,1} + [-A_{22}\cos(A_0) + A_{32}\sin(A_0)]I_{x,1} - [A_{32}\cos(A_0) + A_{22}\sin(A_0)]I_{x,2}$
L	$2A_{12}\cos(A_0)I_{z,2} + 2A_{12}\sin(A_0)I_{z,1} + [-A_{22}\cos(A_0) + A_{32}\sin(A_0)]I_{x,1} - [A_{32}\cos(A_0) + A_{22}\sin(A_0)]I_{x,2}$
M	$-2A_{12}\cos(A_0)I_{z,2} + 2A_{12}\sin(A_0)I_{z,1} + [A_{22}\cos(A_0) - A_{32}\sin(A_0)]I_{y,1} - [A_{32}\cos(A_0) + A_{22}\sin(A_0)]I_{y,2}$
N	$-2A_{12}\cos(A_0)I_{z,2} + 2A_{12}\sin(A_0)I_{z,1} + [A_{22}\cos(A_0) - A_{32}\sin(A_0)]I_{y,1} - [A_{32}\cos(A_0) + A_{22}\sin(A_0)]I_{y,2}$
O	$2A_{11}\cos(\frac{3b}{8})I_{z,2} - 2A_{11}\sin(\frac{3b}{8})I_{z,1} + [A_{21}\cos(\frac{3b}{8}) + A_{31}\sin(\frac{3b}{8})]I_{x,1} + [-A_{21}\sin(\frac{3b}{8}) + A_{31}\cos(\frac{3b}{8})]I_{x,2}$
P	$2A_{11}\cos(\frac{3b}{8})I_{z,2} - 2A_{11}\sin(\frac{3b}{8})I_{z,1} + [A_{21}\cos(\frac{3b}{8}) + A_{31}\sin(\frac{3b}{8})]I_{x,1} + [-A_{21}\sin(\frac{3b}{8}) + A_{31}\cos(\frac{3b}{8})]I_{x,2}$
	$A_0 = b - 2c + d$, $A_{11} = \frac{2a\sinh[\frac{1}{8}\sqrt{-16a^2-9b^2}]}{\sqrt{-16a^2-9b^2}}$, $A_{21} = \cosh[\frac{1}{8}\sqrt{-16a^2-9b^2}]$, $A_{31} = \frac{3b\sinh[\frac{1}{8}\sqrt{-16a^2-9b^2}]}{\sqrt{-16a^2-9b^2}}$
	$A_{12} = \frac{2asinh[\frac{1}{8}\sqrt{-16a^2-(b-d)^2}]}{\sqrt{-16a^2-(b-d)^2}}$, $A_{22} = \sinh[\frac{1}{8}\sqrt{-16a^2-(b-d)^2}]$, $A_{32} = \frac{(b-d)\sinh[\frac{1}{8}\sqrt{-16a^2-(b-d)^2}]}{\sqrt{-16a^2-(b-d)^2}}$
	$a = 3\frac{\omega_Q}{\omega_{RF}}$, $b = 4(3A-\tau)\omega_Q$, $c = -4(3\alpha+\tau)\omega_Q$, $d = 8\tau\omega_Q$.

In this table $2\omega_{RF}\alpha = \frac{\pi}{2}$ where 2α is the $\frac{\pi}{2}$ pulse width, ω_Q is the quadrupolar coupling constant and we have set $\frac{\gamma\hbar B_0}{kT} = 1$.

Similarly, for the magic echo cycles that refocus the magnetization on the $+y$ axis relative to the receiver we have

$$\rho_{Y\text{Total}} = \rho_{\text{C}} + \rho_{\text{D}} + \rho_{\text{I}} + \rho_{\text{J}} - \rho_{\text{A}} - \rho_{\text{B}} - \rho_{\text{M}} - \rho_{\text{N}} \tag{15}$$

and the total density matrix in the $+Y$ direction reduces to

$$\begin{aligned}\rho_{Y\text{Total}} = &\left[-4A_{21}\cos\left(\frac{3b}{8}\right) - 4A_{33}\cos\left(\frac{b}{8}\right) - 4A_{33}\cos\left(\frac{2c}{8}\right)\right.\\ &-4A_{33}\cos\left(\frac{d}{8}\right) - 4A_{31}\sin\left(\frac{3b}{8}\right) + 4A_{32}\sin\left(\frac{b}{8}\right)\\ &\left.-4A_{32}\sin\left(\frac{c}{4}\right) + 4A_{32}\sin\left(\frac{d}{8}\right)\right]I_{y,1}\\ &+\left[-4A_{21}\sin\left(\frac{3b}{8}\right) + 4A_{33}\sin\left(\frac{b}{8}\right) - 4A_{33}\sin\left(\frac{2c}{8}\right)\right.\\ &+4A_{33}\sin\left(\frac{d}{8}\right) + 4A_{31}\cos\left(\frac{3b}{8}\right) + 4A_{32}\cos\left(\frac{b}{8}\right)\\ &\left.-4A_{32}\cos\left(\frac{c}{4}\right) + 4A_{32}\cos\left(\frac{d}{8}\right)\right]I_{y,2}\end{aligned} \tag{16}$$

where A_{21}, A_{31}, A_{32} and A_{33} are again given in Table 4.

It is important to note that the total density matrix in x direction has only one deleterious term $I_{x,2}$ while the y direction has $I_{y,2}$. The weight of deleterious terms are small compared to the desirable terms $I_{x,1}$ or $I_{y,1}$. For instance, when $\omega_{\text{Q}} = 125$ kHz, $\tau = 100$ μs a pulse $\pi/2$ pulse width of $2\alpha = 2$ μs generates deleterious terms $I_{x,2}$ and $I_{y,2}$ that are approximately 2 orders of magnitude smaller than the desired terms $I_{x,1}$ and $I_{y,1}$. The phase cycling scheme shown in Table 1 is based on the CYCLOPS phase cycle developed by Hoult and Richards and is also robust in suppressing ring-down effects of the last pulse, in addition to a variety of errors associated with imbalances in the receiver channels and imperfect $\pi/2$ pulses [13].

Next, we consider the first order term of the Magnus expansion and discuss the higher convergence of the magic echo cycle as compared to the conventional quadrupolar echo sequence. Following the same development for the zeroth order term of the Magnus expansion, the first order term is given by [1]

$$\overline{H}^{1}_{\text{int}} = \frac{-i}{2t_c}\int_0^{t_c}[\widetilde{H}_{\text{int}}(\tau), \int_0^{\tau}\widetilde{H}_{\text{int}}(\phi)\,\mathrm{d}\phi]\,\mathrm{d}\tau \tag{17}$$

which we have rewritten as

$$\overline{H}^{1}_{\text{int}} = \frac{-i}{2t_c}[T_0 + T_1 + T_2 + \ldots.] \tag{18}$$

For the magic echo sequence cycle A, the toggling frame quadrupolar Hamiltonian during each stage of the cycle shown in Fig. 1 is given in Table 1. The different terms in the sum have been computed as follows

$$T_0 = \int_0^{\tau-2\alpha}\int_0^{t_1}[\widetilde{H}_1, \widetilde{H}_1]\,\mathrm{d}t_1\,\mathrm{d}t_0 = 0 \tag{19}$$

$$\begin{aligned}T_1 &= \int_{\tau-2\alpha}^{\tau}\int_0^{\tau-2\alpha}[\widetilde{H}_2.\widetilde{H}_1 - \widetilde{H}_1.\widetilde{H}_2]\,\mathrm{d}t_2\,\mathrm{d}t_1\\ &= -\frac{18i(-2+\sqrt{2})\alpha^2\omega_{\text{Q}}^2}{\pi}I_{x,1}\end{aligned} \tag{20}$$

$$\begin{aligned}T_2 &= \int_{\tau}^{2\tau-\alpha}\int_0^{\tau-2\alpha}[\widetilde{H}_3.\widetilde{H}_1 - \widetilde{H}_1.\widetilde{H}_3]\,\mathrm{d}t_3\,\mathrm{d}t_1\\ &+\int_{\tau}^{2\tau-\alpha}\int_{\tau-2\alpha}^{\tau}[\widetilde{H}_3.\widetilde{H}_2 - \widetilde{H}_2.\widetilde{H}_3]\,\mathrm{d}t_3\,\mathrm{d}t_2\\ &= -\frac{18i(2+\sqrt{2})\alpha^2\omega_{\text{Q}}^2}{\pi}I_{x,1}\end{aligned} \tag{21}$$

$$\begin{aligned}T_3 &= \int_{2\tau-\alpha}^{2\tau+\alpha}\int_0^{\tau-2\alpha}[\widetilde{H}_4.\widetilde{H}_1 - \widetilde{H}_1.\widetilde{H}_4]\,\mathrm{d}t_4\,\mathrm{d}t_1\\ &+\int_{2\tau-\alpha}^{2\tau+\alpha}\int_{\tau-2\alpha}^{\tau}[\widetilde{H}_4.\widetilde{H}_2 - \widetilde{H}_2.\widetilde{H}_4]\,\mathrm{d}t_4\,\mathrm{d}t_2\\ &+\int_{2\tau-\alpha}^{2\tau+\alpha}\int_{\tau}^{2\tau-\alpha}[\widetilde{H}_4.\widetilde{H}_3 - \widetilde{H}_3.\widetilde{H}_4]\,\mathrm{d}t_4\,\mathrm{d}t_3\\ &= \frac{36}{\pi}i\alpha^2\omega_{\text{Q}}^2 I_{z,1} + \frac{36\sqrt{2}}{\pi^2}i\alpha^2\omega_{\text{Q}}^2 I_{y,1}\\ &+\frac{36(-\sqrt{2}+\pi)}{\pi^2}i\alpha^2\omega_{\text{Q}}^2 I_{x,1}\end{aligned} \tag{22}$$

$$\begin{aligned}T_4 = &\int_{2\tau+\alpha}^{4\tau}\int_0^{\tau-2\alpha}[\widetilde{H}_5.\widetilde{H}_1 - \widetilde{H}_1.\widetilde{H}_5]\,\mathrm{d}t_5\,\mathrm{d}t_1\\ &+\int_{2\tau+\alpha}^{4\tau}\int_{\tau-2\alpha}^{\tau}[\widetilde{H}_5.\widetilde{H}_2 - \widetilde{H}_2.\widetilde{H}_5]\,\mathrm{d}t_5\,\mathrm{d}t_2\\ &+\int_{2\tau+\alpha}^{4\tau}\int_{\tau}^{2\tau-\alpha}[\widetilde{H}_5.\widetilde{H}_3 - \widetilde{H}_3.\widetilde{H}_5]\,\mathrm{d}t_5\,\mathrm{d}t_3\\ &+\int_{2\tau+\alpha}^{4\tau}\int_{2\tau-\alpha}^{2\tau+\alpha}[\widetilde{H}_5.\widetilde{H}_4 - \widetilde{H}_4.\widetilde{H}_5]\,\mathrm{d}t_5\,\mathrm{d}t_4 = 0\end{aligned} \tag{23}$$

$$\begin{aligned}T_5 = &\int_{4\tau}^{6\tau-\alpha}\int_0^{\tau-2\alpha}[\widetilde{H}_6.\widetilde{H}_1 - \widetilde{H}_1.\widetilde{H}_6]\,\mathrm{d}t_6\,\mathrm{d}t_1\\ &+\int_{4\tau}^{6\tau-\alpha}\int_{\tau-2\alpha}^{\tau}[\widetilde{H}_6.\widetilde{H}_2 - \widetilde{H}_2.\widetilde{H}_6]\,\mathrm{d}t_6\,\mathrm{d}t_2\\ &+\int_{4\tau}^{6\tau-\alpha}\int_{\tau}^{2\tau-\alpha}[\widetilde{H}_6.\widetilde{H}_3 - \widetilde{H}_3.\widetilde{H}_6]\,\mathrm{d}t_6\,\mathrm{d}t_3\\ &+\int_{4\tau}^{6\tau-\alpha}\int_{2\tau-\alpha}^{2\tau+\alpha}[\widetilde{H}_6.\widetilde{H}_4 - \widetilde{H}_4.\widetilde{H}_6]\,\mathrm{d}t_6\,\mathrm{d}t_4\\ &+\int_{4\tau}^{6\tau-\alpha}\int_{2\tau+\alpha}^{4\tau}[\widetilde{H}_6.\widetilde{H}_5 - \widetilde{H}_5.\widetilde{H}_6]\,\mathrm{d}t_6\,\mathrm{d}t_5 = 0\end{aligned} \tag{24}$$

$$
\begin{aligned}
T_6 = & \int_{6\tau-\alpha}^{6\tau+\alpha}\int_{0}^{\tau-2\alpha}[\widetilde{H}_7.\widetilde{H}_1-\widetilde{H}_1.\widetilde{H}_7]\,dt_7\,dt_1 \\
& + \int_{6\tau-\alpha}^{6\tau+\alpha}\int_{\tau-2\alpha}^{\tau}[\widetilde{H}_7.\widetilde{H}_2-\widetilde{H}_2.\widetilde{H}_7]\,dt_7\,dt_2 \\
& + \int_{6\tau-\alpha}^{6\tau+\alpha}\int_{\tau}^{2\tau-\alpha}[\widetilde{H}_7.\widetilde{H}_3-\widetilde{H}_3.\widetilde{H}_7]\,dt_7\,dt_3 \\
& + \int_{6\tau-\alpha}^{6\tau+\alpha}\int_{2\tau-\alpha}^{2\tau+\alpha}[\widetilde{H}_7.\widetilde{H}_4-\widetilde{H}_4.\widetilde{H}_7]\,dt_7\,dt_4 \\
& + \int_{6\tau-\alpha}^{6\tau+\alpha}\int_{2\tau+\alpha}^{4\tau}[\widetilde{H}_7.\widetilde{H}_5-\widetilde{H}_5.\widetilde{H}_7]\,dt_7\,dt_5 \\
& + \int_{6\tau-\alpha}^{6\tau+\alpha}\int_{4\tau}^{6\tau-\alpha}[\widetilde{H}_7.\widetilde{H}_6-\widetilde{H}_6.\widetilde{H}_7]\,dt_7\,dt_6 \\
= & -\frac{36}{\pi}i\alpha^2\omega_Q^2 I_{z,1}+\frac{36\sqrt{2}}{\pi^2}i\alpha^2\omega_Q^2 I_{y,1} \\
& -\frac{36(\sqrt{2}+\pi)}{\pi^2}i\alpha^2\omega_Q^2 I_{x,1} \qquad (25)
\end{aligned}
$$

$$
\begin{aligned}
T_7 = & \int_{6\tau+\alpha}^{7\tau}\int_{0}^{\tau-2\alpha}[\widetilde{H}_8.\widetilde{H}_1-\widetilde{H}_1.\widetilde{H}_8]\,dt_8\,dt_1 \\
& + \int_{6\tau+\alpha}^{7\tau}\int_{\tau-2\alpha}^{\tau}[\widetilde{H}_8.\widetilde{H}_2-\widetilde{H}_2.\widetilde{H}_8]\,dt_8\,dt_2 \\
& + \int_{6\tau+\alpha}^{7\tau}\int_{\tau}^{2\tau-\alpha}[\widetilde{H}_8.\widetilde{H}_3-\widetilde{H}_3.\widetilde{H}_8]\,dt_8\,dt_3 \\
& + \int_{6\tau+\alpha}^{7\tau}\int_{2\tau-\alpha}^{2\tau+\alpha}[\widetilde{H}_8.\widetilde{H}_4-\widetilde{H}_4.\widetilde{H}_8]\,dt_8\,dt_4 \\
& + \int_{6\tau+\alpha}^{7\tau}\int_{2\tau+\alpha}^{4\tau}[\widetilde{H}_8.\widetilde{H}_5-\widetilde{H}_5.\widetilde{H}_8]\,dt_8\,dt_5 \\
& + \int_{6\tau+\alpha}^{7\tau}\int_{4\tau}^{6\tau-\alpha}[\widetilde{H}_8.\widetilde{H}_6-\widetilde{H}_6.\widetilde{H}_8]\,dt_8\,dt_6 \\
& + \int_{6\tau+\alpha}^{7\tau}\int_{6\tau-\alpha}^{6\tau+\alpha}[\widetilde{H}_8.\widetilde{H}_7-\widetilde{H}_7.\widetilde{H}_8]\,dt_8\,dt_7 \\
= & \frac{18(\sqrt{2}+2)}{\pi}i\alpha^2\omega_Q^2 I_{x,1} \qquad (26)
\end{aligned}
$$

Summing all eight terms of the integral, the first order term of the Magnus expansion for magic echo cycle A reduces to

$$
\overline{H}^1_{\mathrm{int}}(\mathrm{ME}) = \frac{1}{7\tau}\frac{\omega_Q^2}{\omega_{RF}^2}\left[\frac{18\sqrt{2}}{8}I_{y,1}-\frac{9}{16}(4\sqrt{2}+(-2+\sqrt{2}))I_{x,1}\right] \qquad (27)
$$

By a similar calculation, using the results for the toggling frame Hamiltonians published in reference [4] for the conventional two pulse sequence, the first order term of the Magnus expansion reduces to

$$
\overline{H}^1_{\mathrm{int}}(\mathrm{SE}) = \frac{B}{3\tau}I_{y,1}-\frac{A}{3\tau}I_{z,1}+\frac{A}{3\tau}I_{x,1} \qquad (28)
$$

where

$$
A = \frac{18\alpha^2\omega_Q^2[\pi(-2+\sin(\frac{\pi\tau}{2\alpha}))+\sin(\frac{\pi\tau}{\alpha})]}{\pi^2} \qquad (29)
$$

and

$$
B = \frac{18\alpha^2\omega_Q^2[1+\cos(\frac{\pi\tau}{\alpha})]}{\pi^2} \qquad (30)
$$

Together with the zeroth order terms of the Magnus expansion, the above results show that the magic echo cycle is more robust compared to the conventional solid echo cycle in refocusing the spin dynamics of quadrupolar spins. The zeroth order term of the Magnus expansion for the conventional two pulse cycle, reported in reference [4] is given by

$$
\overline{H}^0_{\omega Q} = \frac{4\alpha\omega_Q}{\pi\tau}(I_{x,2}-I_{y,2}) \qquad (31)
$$

Setting the cycle time, 7τ, of the magic echo cycle equal to that of the conventional two pulse cycle, 3τ, the zeroth order term of the Magnus expansion for a magic echo given in Eq. (7) is the same magnitude as that given in the expression above. However, the zeroth order term of the Magnus expansion for the conventional cycle contains a sum of two terms, $I_{x,2}-I_{y,2}$, whereas that of the magic echo only contains one which does not commute with the equilibrium state, $I_{z,1}$. Hence, the dynamics are more complex for a given value of α for the conventional two pulse cycle. In addition, the first order term of the Magnus expansion for a magic echo is much smaller than that of the two pulse conventional cycle. For example, with a pulse width of $2\alpha = 2.0\ \mu s$, $\omega_Q = 125\ kHz$, and equal evolution times $\tau = 100\ \mu s$ and $\tau = 300\ \mu s$ for the magic echo and the solid echo, respectively, the first order terms reduce to

$$
\overline{H}^1_{\mathrm{int}}(\mathrm{ME}) = 103.22I_{x,1}+115.14I_{y,1} \qquad (32)
$$

and

$$
\overline{H}^1_{\mathrm{int}}(\mathrm{SE}) = -198.94I_{x,1}+63.32I_{y,1}-198.94I_{z,1} \qquad (33)
$$

in units of Hertz. With stronger RF power and shorter pulse spacings, the first order term of the Magnus expansion for the magic echo can be further reduced compared to that of the conventional two pulse cycle. Consequently, the magic echo cycle is a more robust sequence for quadrupolar echo spectroscopy of solids compared to the conventional two pulse quadrupolar echo sequence.

Considering Fig. 1, the magic echo cycle also performs a π rotation and hence refocuses chemical shift and static field inhomogeneity simultaneous with the quadrupolar interaction. Previous work associated with refocussing the chemical shift and static field inhomogeneity with the first order quadrupolar interaction in spin-1 quadrupolar echo spectroscopy using a modified version of the conventional cycle shown in Fig. 2, has been reported and described by Antonijevic et al. [14]. Their work showed a phase cycling scheme that also yields less distorted spectra than the conventional quadrupolar echo sequence. Other cycles developed for refocusing chemical shift and static field inhomogeneity with the quadrupolar interaction have also been reported by Siminovich [15]. To show that the magic echo cycles outlined here refocus the effects of static field inhomogeneity and chemical shift, we assume a Hamiltonian $H = \Delta\omega I_{z,1}$ and compute

the zeroth order term of the Magnus expansion. For cycle A, shown in Fig. 1

$$\overline{H}^{0}_{\Delta\omega}(\mathrm{ME}) = \frac{-4}{7\tau}\frac{\Delta\omega}{\omega_{\mathrm{RF}}}I_{x,1} + \frac{2}{7\tau}\frac{\Delta\omega}{\omega_{\mathrm{RF}}}I_{y,1} + \frac{2}{7\tau}\frac{\Delta\omega}{\omega_{\mathrm{RF}}}[\omega_{\mathrm{RF}}(\tau-2\alpha)+2\cos[\omega_{\mathrm{RF}}(2\tau-\alpha)]-1]I_{z,1} \tag{34}$$

where we have used the following constraints:

$$2\omega_{\mathrm{RF}}\alpha = \frac{\pi}{2} \tag{35}$$

and

$$(2\tau-\alpha)\omega_{\mathrm{RF}} = n\pi, \quad n = 1,2,3,\ldots \tag{36}$$

For the solid echo cycle shown in Fig. 2 the zeroth order term for the chemical shift or static field inhomogeneity is

$$\overline{H}^{0}_{\Delta\omega}(\mathrm{SE}) = \frac{1}{3\tau}[-aI_{x,1} + bI_{y,1} + aI_{z,1}] \tag{37}$$

where

$$a = 2\Delta\omega\left[\left(\frac{4}{\pi}-1\right)\alpha+\tau\right] \tag{38}$$

and

$$b = 2\Delta\omega\left[2\left(\frac{4}{\pi}-1\right)\alpha+\tau\right] \tag{39}$$

In cases where the ω_{RF} is made larger than $\Delta\omega$, the zeroth order term of the Magnus expansion for the offset Hamiltonian with the magic echo sequence can be made negligible. In this situation, the magic echo pulse sequence refocuses static field inhomogeneity and chemical shift effects completely. This is not the case with the conventional two pulse sequence, and as a consequence it does not refocus the effects of static field inhomogeneity and chemical shift even for strong RF pulses.

3. Experimental results

We tested the improved performance of a magic echo over the two pulse conventional cycle on a deuterated sample of polyethene. The experiments were performed on a Tecmag Apollo solid state NMR system with a homebuilt NMR probe operating at 26.75 MHz. The coil in our NMR probe had an inner diameter of approximately 2 mm, consisted of 6 turns of 30 AWG copper wire and had a geometry that is known for producing a homogeneous field in the center of the sample [16]. The deuterated polyethelene sample was purchased from Polymer Source, Inc. located in Montreal, Canada. The experimental procedure for setting up the experiments involved putting the system at resonance and tuning the $\pi/2$ pulses using well known techniques in solid state NMR on a sample of deuterated water [17]. In the experiments, the dwell time was set to 0.5 μs, a recycle delay of 10 s was used and 50,000 scans were collected at room temperature. The two pulse cycle used an 8-step phase cycling scheme that has been shown to cancel deleterious finite pulse width artifacts to first order of the Magnus expansion [4]. The spectra acquired with a magic echo used the 16-step phase cycling scheme given in Table 1.

Fig. 3 highlights the experimental results of a quadrupolar echo acquired with the conventional two pulse cycle and a magic echo cycle for a $\pi/2$ pulse length of 1.3 μs and 1.8 μs. In the experiments, the tau spacings were set to 104.65 μs for the magic echo and 312.3 μs for the conventional two pulse sequence. This ensures that the complete evolution time following the first excitation pulse is made the same, so that in both experiments the spin system evolves under the quadrupolar interaction and irreversible relaxation not refocused by the RF pulses for an equal amount of time. The results highlight that the peak signal to noise is larger by a factor of approximately 2 in the magic echo over the solid echo for a 1.3 μs pulse (referring to Fig. 3A and B). In addition, the signal to noise in the tail ends of the quadrupolar pattern is larger by a factor of approximately 5 in the case of a magic echo compared to the conventional two pulse quadrupolar echo for this pulse power. This behavior is expected as discussed in the theoretical section. The zeroth order term of the Magnus expansion for a Magic echo contains only one term that does not commute with $I_{z,1}$, whereas the two pulse conventional cycle contains two terms (refer to Eq. (7) and Eq. (31)), making the dynamics much more complex for a given value of α. Comparing the first order terms of the Magnus expansion for 1.3 μs $\pi/2$ pulses, the first order term for the conventional two pulse cycle contains 3 operators that are larger than that of the magic echo cycle which only contains 2 operators. As a consequence, the magic echo cycle is more robust in refocusing the spin dynamics of spin-1 quadrupolar nuclei and yields better looking spectra.

For a longer $\pi/2$ pulse equal to 1.8 μs, the experimental data show that the magic echo cycle produces approximately the same peak signal to noise as the conventional quadrupolar echo cycle. However, the outer edges of the spectra appear to be better resolved with the magic echo compared to the conventional two pulse cycle. This is also well predicted by the theoretical analysis presented in the last section. Again, both the zeroth order and first order terms of the Magnus expansion for the magic echo are smaller than that of the conventional two pulse cycle.

Referring again to Fig. 3A and B, the magic echo cycle also produces a higher signal in the central peak of the spectrum compared to the two pulse solid echo. This peak is due to a highly mobile group of the sample, where the quadrupolar interaction is partially averaged away due to molecular motion, and has been observed by others in a similar sample [18]. These results are also in good agreement with what was shown in the theoretical work outlined, in that the magic echo cycle refocuses chemical shift and static field inhomogeneity whereas the conventional two pulse echo does not. Lastly, we found that the requirement we imposed on the spin locking field for a

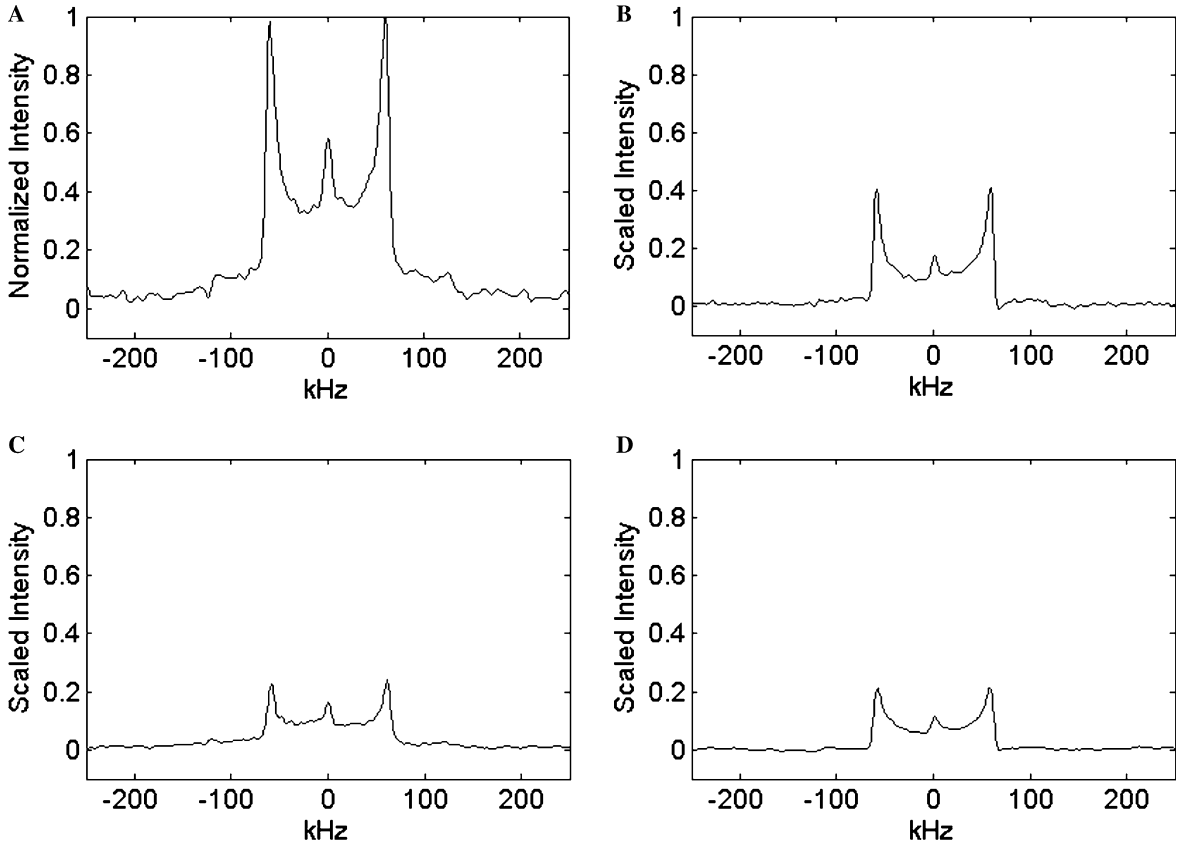

Fig. 3. Experimental data highlighting the quadrupolar echo spectra of deuterated polyethelene acquired with a magic echo using $\pi/2$ pulse widths of (A) 1.3 μs and (C) 1.8 μs and a conventional quadrupolar cycle using $\pi/2$ pulse widths of (B) 1.3 μs and (D) 1.8 μs. Figures B, C and D have all been scaled relative to the maximum intensity of that in (A), and the phase cycling implemented is discussed in the text. This figure shows that when 1.3 μs $\pi/2$ pulses are implemented, the signal to noise of a magic echo shown in (A) is larger by approximately a factor of 2 in the peaks and approximately 5 in the tail ends of the spectrum, compared to that of the conventional two pulse quadrupolar cycle shown in (B). For 1.8 μs $\pi/2$ pulses, the peak signal to noise for the two cycles is approximately the same, though the magic echo resolves the tail ends of the powder pattern clearer. For both pulse widths, the center peak of the signal of a magic echo is larger compared to the center peak of the signal of the conventional two pulse cycle, due to the refocusing of chemical shift and static field inhomogeneity.

magic echo cycle, $2\tau - \alpha = n\pi$, did not directly affect any of the experimental data. We believe that this might be due to the fact that the entire zeroth order term scales as $1/\omega_{RF}$ and any change in the sin or cosine terms shown in the toggling frame Hamiltonians of Table 2 are negligible compared to the relative size of the RF field.

4. Conclusions

Cycles for performing echo spectroscopy of spin-1 nuclei in the presence of a quadrupolar interaction, chemical shift interaction and static field inhomogeneity with a magic echo are presented. A phase cycling scheme is introduced, via the formalism of average Hamiltonian theory, for suppressing deleterious finite pulse width artifacts. With the proper phase cycling and sufficient RF power, magic echo based quadrupolar echo spectra yield a higher signal to noise over the familiar two pulse quadrupolar echo cycle due to higher convergence in the Magnus expansion and the simultaneous refocusing of chemical shift, static field inhomogeneity and quadrupolar interactions. Experiments on deuterated polyethelene indicate an enhancement of approximately 2 in peak signal to noise and approximately 5 in the tail ends of the powder pattern. It is expected that the magic echo cycles reported here will be useful for a broad range of applications of quadrupolar echo spectroscopy of polymers, and other solid and semisolid systems.

Acknowledgment

E.S. Mananga acknowledges support by The City University of New York Graduate Center Alliances for Graduate Education in the Professoriate (AGEP) program funded by the National Science Foundation. Y.S. Rumala thanks the Department of Education McNair Scholars program as well as the National Science Foundation Louis Stokes Alliance for Minority Participation program for their support.

References

[1] U. Haeberlen, J.S. Waugh, Coherent averaging effects in magnetic resonance, Phys. Rev. 175 (1968) 453–467.
[2] M.H. Levitt, D. Suter, R.R. Enrst, Composite pulse excitation in three-level systems, J. Chem. Phys. 80 (1984) 3064–3068.

[3] D.J. Siminovich, D.P. Raleigh, E.T. Olejniczak, R.G. Griffen, Composite pulse excitation in quadrupole echo spectroscopy, J. Chem. Phys. 84 (1986) 2556–2565.
[4] E.S. Mananga, Y.S. Rumala, G.S. Boutis, Finite pulse width artifact supression in spin-1 quadrupolar echo spectra by phase cycling, J. Magn. Reson. 181 (2006) 296–303.
[5] W.-K. Rhim, A. Pines, J.S. Waugh, Time-reversal experiments in dipolar-coupled spin systems, Phys. Rev. B 3 (1971) 684–696.
[6] S. Matsui, Solid-state NMR imaging by magic sandwich echoes, Chem. Phys. Lett. 179 (1991) 684–696.
[7] S. Matsui, Y. Ogasawara, T. Inouye, Proton images of elastomers by solid-state NMR imaging, J. Magn. Reson. A 105 (1993) 215–218.
[8] S. Matsui, A. Uraoka, T. Inouye, Solid-state NMR imaging by tetrahedral-magic-echo time-suspension sequences, J. Magn. Reson. A. 120 (1996) 11–17.
[9] W. Zhang, D.G. Cory, First direct measurement of the spin diffusion rate in a homogeneous solid, Phys. Rev. Lett. 80 (1998) 1324–1327.
[10] G.S. Boutis, D. Greenbaum, H. Cho, D.G. Cory, C. Ramanathan, Spin diffusion of correlated two spin states in a dielectric crystal, Phys. Rev. Lett. 92 (2004) 107–109.
[11] G.S. Boutis, P. Capellaro, H. Cho, C. Ramanathan, D.G. Cory, Pulse error compensating symmetric magic echo trains, J. Magn. Reson. 161 (2003) 132–137.
[12] S. Vega, A. Pines, Operator formalism for double quantum NMR, J. Chem. Phys. 66 (1977) 5624–5644.
[13] D.I. Hoult, R.E. Richards, Critical factors in the design of sensitive high resolution nuclear magnetic resonance spectrometers, Proc. R. Soc. Lond. Series A 344 (1975) 311–340.
[14] S. Antonijevic, S. Wimperis, Refocussing of chemical and paramagnetic shift anisotropies in ^{2}H NMR using the quadrupolar echo experiment, J. Magn. Res. 164 (2003) 343–350.
[15] D.J. Siminovitch, M. Rance, K.R. Jeffrey, M.F. Brown, The quadrupolar spectrum of spin $I = 1$ in a lipid bilayer in the presence of paramagnetic ions, J. Magn. Res. 58 (1984) 62–75.
[16] S. Idziak, U. Haeberlen, Design and construction of a high homogeneity RF coil for solid-state multiple pulse NMR, J. Magn. Reson. 50 (1982) 281–288.
[17] B.C. Gerstein, C.R. Dybowski, Transient Techniques in NMR of Solids. An Introduction to Theory and Practice, Academic Press, Orlando, 1985.
[18] P.M. Henrichs, J.M. Hewitt, M. Linder, Experimental aspects of deuterium NMR of solids, J. Magn. Reson. 60 (1984) 280–298.